Published in final edited form as:
Dev Dyn. 2012 November ; 241(11): 1678–1694. doi:10.1002/dvdy.23855.

A Comprehensive Timeline of Mesodermal Development in the Quail Small Intestine

Rebecca T. Thomason[1], **David M. Bader**[1,2,*], and **Nichelle I. Winters**[1]

[1]Department of Cell and Developmental Biology, Vanderbilt University, Nashville, TN, USA

[2]Department of Medicine, Vanderbilt University, Nashville, TN, USA

Abstract

Background—To generate the mature intestine, splanchnic mesoderm diversifies into six different tissue layers each with multiple cell types through concurrent and complex morphogenetic events. Hindering the progress of research in the field is the lack of a detailed description of the fundamental morphological changes that constitute development of the intestinal mesoderm.

Results—We utilized immunofluorescence and morphometric analyses of wild type and Tg(*tie1*:H2B-eYFP) quail embryos to establish a comprehensive timeline of mesodermal development in the avian intestine. The following landmark features were analyzed from appearance of the intestinal primordium through generation of the definitive structure: radial compartment formation, basement membrane dynamics, mesothelial differentiation, mesenchymal expansion and growth patterns, smooth muscle differentiation, and maturation of the vasculature. In this way, structural relationships between mesodermal components were identified over time.

Conclusions—This integrated analysis presents a roadmap for investigators and clinicians to evaluate diverse experimental data obtained at individual stages of intestinal development within the longitudinal context of intestinal morphogenesis.

Keywords

quail; small intestine; splanchnic mesoderm; mesenchyme

Introduction

Intestinal disorders affect a large number of individuals in both pediatric and adult settings. Many of these conditions including intestinal atresia, motility disorders, Hirschprung's disease, and gastrointestinal stromal tumors (GIST) have multiple and incompletely understood etiologies (Louw and Barnard, 1955; Mazur and Clark, 1983; Sanders, 1996; Hirota et al., 1998; Newgreen and Young, 2002; Heanue and Pachnis, 2007; Streutker et al., 2007; Appelman, 2011; Guzman et al., 2011). One of the difficulties in deciphering the mechanisms underlying these diseases is the lack of information available on the development of a major component of the gut tube—the intestinal mesoderm. Understanding development of the mesoderm is essential for a complete picture of the mechanisms leading to congenital as well as adult intestinal disorders.

*Corresponding Author: David M. Bader, 2220 Pierce Ave, 348 PRB, Nashville, TN 37232-6300, Fax: 615-936-3527, Phone: 615-936-1976, david.bader@vanderbilt.edu.

A description of the structure of the adult intestine reveals the complexity of the mesodermal tissues generated in the embryo. The innermost layer, the mucosal epithelium, is comprised primarily of columnar epithelial cells resting on a basement membrane. Supporting the mucosal epithelium is a mesenchymal core called the lamina propria, which is composed of a capillary plexus, lymphatic vessels, nerves, myofibroblasts and fibroblasts. The lamina propria and mucosal epithelium are arranged into fingerlike projections, called villi, protruding into the lumen of the intestine. External to the mucosal epithelium, minor variations in structure are observed between the avian and mammalian intestine. The adult chick intestine lacks a submucosal connective tissue layer and muscularis mucosa. Instead, there are four concentric visceral smooth muscle cell layers that begin just subjacent to the lamina propria and are positioned outwardly in the following order: inner longitudinal, inner circular, outer circular and outer longitudinal (Gabella, 1985; Yamamoto, 1996). The inner longitudinal muscle layer of the avian is analogous to the mammalian muscularis mucosa. The circular muscle layer of mammals including mice and humans can also be divided into two layers due to structural differences though is often referred to singularly (Eddinger, 2009). Thus, the most significant variation between the mammalian and avian intestine is the presence or absence of a submucosal connective tissue layer. The large blood vessels of the chick intestine reside within or just deep to the thin outer longitudinal visceral smooth muscle cell layer and extend circumferentially. Vascular branches dive deep into the intestinal layers to eventually supply the endothelial plexus of the villi (Jacobson and Noer, 1952). The enteric neuronal network is divided into two main regions: the first adjacent to the large blood vessels described above that reside near the surface and the second between the inner circular and inner longitudinal smooth muscle layers (Gabella, 1985). Finally, at the coelomic surface is a serosal membrane composed of a flat sheet of epithelial cells called mesothelium with an underlying basement membrane and thin connective tissue layer (Fig. 1).

On first examination, the embryonic intestinal primordium offers only hints of its eventual elaborate structure. After gastrulation in the avian embryo, the lateral plate mesoderm splits into splanchnic and somatic mesoderm bilaterally generating a right and left coelomic cavity between the two layers. The splanchnic mesoderm, underlying endoderm, and an intervening endothelial plexus compose the intestinal anlage and are initially organized as a flat sheet (Fig. 1 A, (Meier, 1980; Pardanaud et al., 1989)). This anlage folds laterally and from the anterior and posterior ends to meet at the ventral midline giving rise to a tube and uniting the right and left lateral cavities into a common coelom (Fig. 1 B, (Wells and Melton, 1999; Zorn and Wells, 2009)). The epithelial endoderm gives rise to the mucosa that lines the villi and intestinal crypts (Coulombre and Coulombre, 1958; Mitjans et al., 1997; Madison et al., 2005; Dauça et al., 2007; Grosse et al., 2011; Spence et al., 2011). The splanchnic mesoderm diversifies to generate the connective tissue, vasculature, smooth muscle and serosal layers (McHugh, 1995; Drake et al., 1997; Hashimoto et al., 1999; Wilm et al., 2005; Kim et al., 2007; Milgrom-Hoffman et al., 2011; Powell et al., 2011; Winters et al., 2012). Migratory neural crest cells invade to form the enteric nervous system and the vascular system organizes from incompletely identified progenitors (Young and Newgreen, 2001; Young et al., 2004; Burns et al., 2009; Nagy et al., 2009). Throughout these processes, the intestine must undergo a dramatic increase in length and diameter herniating outside of the body cavity to accommodate its tremendous growth (Savin et al., 2011). Thus, cells of all three germ layers must coordinate invasion, migration, differentiation, growth, and tissue morphogenesis to generate the mature intestinal structure.

Despite comprising the majority of the adult intestine, development of the mesoderm is poorly described relative to the more extensively studied endodermal and neuronal components. Within the mesoderm, multiple cellular types and tissue layers develop in concert. Most studies are focused on the differentiation of a specific cell type during a

narrow developmental window. Furthermore, studies utilize a variety of model organisms. Thus, assembling the available data distributed within the literature into a basic timeline of the major morphological changes that occur during intestinal development is extremely difficult. Knowledge of the temporal and spatial relationships of developmental events in the intestine is essential to design experiments and interpret data.

We sought to establish a comprehensive timeline of the major events in intestinal mesoderm development from the first appearance of the intestinal anlage to formation of the definitive structure in a single species. Quail embryos were selected due to their availability in large quantities, emerging transgenic models, and the ability to easily time their development with precision (Huss et al., 2008). Additionally, small intestine development has not been described in the quail (Coulombre and Coulombre, 1958; Grey, 1972; Gabella, 1985; Yamamoto, 1996; Hashimoto et al., 1999; Hiramatsu and Yasugi, 2004; Kim et al., 2007; Mao et al., 2010). Importantly, the major structural features of the avian intestine, with the above noted variations, correspond with the mammalian intestine and thus the information obtained from studies of the avian embryo is widely applicable. We describe landmark features of intestinal mesoderm formation throughout embryogenesis that if analyzed at any single stage, provide an inclusive snapshot of the status of mesodermal development. Furthermore, through this integrated approach, we identified pivotal developmental time points at which key processes occur simultaneously. These data provide the field with the fundamental developmental and morphological guideposts in intestinal mesoderm development upon which variation in organogenesis caused by genetic, experimental and surgical intervention can be compared and further analyzed.

Results

Establishment and maturation of the major intestinal compartments

As described above, the adult avian intestine has seven concentric tissue layers, six of which are derived from the splanchnic mesoderm. However, there are only two continuous basement membranes within the intestine (one below the mucosal epithelium and the other subjacent to the outer serosal mesothelium) that divide the seven layers into three compartments: the mucosa, the middle connective and muscular tissue (largest component), and the outer serosa (Simon-Assmann et al., 1995; Lefebvre et al., 1999). The intestinal primordium, similar to the adult structure, is divided by two basement membranes (black lines) into three compartments: endoderm (En), mesenchyme/mesenchymal space, and mesoderm/outer epithelium (SpM) (Fig. 1 A). While subsequent morphogenetic events will greatly increase the complexity of cell and tissue relationships, the arrangement of these basement membranes represent one of the few histological similarities between the embryonic and adult intestine (Fig. 1).

To determine whether this basic structural relationship is maintained throughout development into adult life, we examined laminin staining throughout development. Laminin is an integral component of basement membranes. At embryonic day 1.9 (E1.9, equivalent to HH12) in the quail embryo, two basement membranes with solid, uninterrupted laminin staining were identified below the endoderm and the splanchnic mesoderm, respectively (Fig. 2 A–B, arrowheads). The basement membranes were distinctly separated along the majority of the medial-lateral axis though they did appear to contact one another at discrete points (Fig. 2 B, arrows). The mesenchymal space was very narrow and sparsely populated with cells (Fig. 2 B, asterisk). At E2.1 (HH14), laminin staining of the outer basement membrane appeared slightly fragmented (white arrowheads) and in limited, sporadic regions, the mesenchymal space contained a single layer of cells (Fig. 2 C–D, asterisks). At E2.2 (HH16) and E3 (HH18), the basement membrane underlying the outer epithelium was well dispersed evidenced by discontinuous laminin staining (Fig. 2 E–F,

white arrowheads; data not shown). There were also multiple cell layers within the mesenchyme (Fig. 2 F, asterisks). At E3.5 (HH21), the anterior and posterior portions of the intestine had folded into a tube while the middle portion remained open ventrally. In both the open and closed regions, the outer epithelial basement membrane had returned to an unbroken configuration (arrowheads) without the large gaps observed in earlier stages (Fig. 2 G–J). Though continuous, the outer basement membrane was still rough in appearance suggesting E3.5 was a transition point to the smooth, unbroken basement membrane observed at E4 (compare Fig. 2 G–J to Fig. 4 E–F).

Between E5 and E6 the gut tube completed ventral closure. At E5 (HH27), the outer epithelial basement membrane was again dispersed (Fig. 3 A–B, white arrowhead) but quickly returned to a continuous configuration by E6 (HH29) (Fig. 3 C–D, white arrowhead). Once solidified at E6, no further changes in the outer epithelial basement membrane were observed through E16. However, the mesenchymal layer underwent dynamic changes over these stages including contributing to villus formation at E10 (Fig. 3 E–F) and mesenchymal compaction and differentiation (Fig. 3 G–H). Additionally at E16, laminin staining in the endodermal basement membrane appeared diffuse (Fig. 3 G–H, yellow arrowhead). Thus, though the outer basement membrane oscillates between discontinuous and continuous states, both basement membranes observed in the intestinal primordium were readily identified throughout development defining the three basic tissue compartments of the intestine.

Development of the outer epithelium

In the adult, the outer epithelium is a simple squamous cell layer, termed mesothelium, that is important for protection of coelomic organs and providing a non-adhesive surface for movement (Mutsaers, 2002; Mutsaers, 2004; Yung and Chan, 2007). We next sought to determine if the periodic dissociation of the outer basement membrane was correlated with differentiation of the outer epithelium into mesothelium. In the embryo and adult, the mesothelium expresses the intermediate filament protein cytokeratin and resides upon a continuous, laminin-enriched basement membrane. A recent lineage tracing study from our laboratory demonstrated that cells within the splanchnic mesoderm of the developing gut tube eventually give rise to the intestinal mesothelium (Winters et al., 2012).

To investigate the development of the outer epithelium, we stained serial sections of quail midgut with antibodies for the epithelial markers cytokeratin and laminin. As described above, the outer epithelium and mesenchyme first appeared as distinct cellular layers at E2.1 (HH14). At this time, the outer epithelium was stratified and the underlying basement membrane was fragmented (see above, Fig. 2 D). At E3.5 (HH21), the outer epithelium remained stratified and was cytokeratin-negative. Laminin staining in the outer basement membrane (arrows) had returned to an unbroken configuration (Fig. 4 A–C). Twelve hours later, at E4 (HH24), the outer epithelium was, for the first time, a single cell layer thick (arrowheads) with very faint staining for cytokeratin (Fig. 4 D–F). At E5 (HH27), we observed more prevalent cytokeratin staining within the outer epithelium despite dispersed laminin staining in the basement membrane (Fig. 4 G–I, arrowheads). Finally, at E6 (HH29) a simple squamous epithelium with robust cytokeratin staining and a continuous basement membrane (arrows) characteristic of the adult mesothelial structure was present throughout the midgut (Fig. 4 J–L). This mature mesothelial configuration was observed throughout the remainder of development. Thus, the transition of the basement membrane to an unbroken conformation at E3.5 was followed shortly by conversion of the outer epithelium from a stratified to simple layer. The subsequent breakdown and solidification of the outer basement membrane at E5-E6 was concurrent with differentiation of the outer cell layer into a mature, cytokeratin positive mesothelium.

Expansion of the mesenchymal compartment

As described in Figure 2 and 3, the mesenchymal compartment underwent a dramatic expansion over these early stages of intestinal development. We next quantified the change in size of the mesenchymal compartment over time to determine if there was any correlation with basement membrane breakdown. We measured the distance between the endoderm and outer epithelial basement membranes at multiple medial-lateral positions to determine the average width of the mesenchymal compartment at each stage. The mesenchymal space at E1.9 (HH12) was narrow, averaging 7.5 μm in width. At E2.1 (HH14), despite the slight increase in the number of cells found in the mesenchymal space at this time, the overall average width was 6.4 μm. Between E2.1-E3.5 (HH14-HH21) the mesenchymal compartment expanded abruptly from 6.4 μm to 103 μm in width. This time period corresponded to the stages over which the outer basement membrane was broken down. Interestingly, after the basement membrane solidified again at E3.5, the distance between the two basement membranes decreased to 74 μm by E4. The second instance of outer basement membrane breakdown at E5 also correlated with a small increase in mesenchymal compartment width though generally the mesenchymal width trended downward between E3.5 and E6 (Fig. 5 A).

Over subsequent stages, the outer basement membrane was solid and the intestinal tube was closed. We next examined mesenchymal cross-sectional area and intestinal length to determine if these variables changed proportionately over time. We quantified mesenchymal cross-sectional area by outlining both the inner and outer basement membranes and calculating the intervening pixels using Metamorph software. We divided the small intestine into quarters along the length of the tube, small intestine (SI) 1–4, and analyzed each region individually at each stage. We also measured the length of the small intestine over the same stages by dissecting away the mesentery and extending the intestine out in a straight line. The anterior regions of the small intestine had consistently larger mesenchymal areas than the posterior regions over all stages examined. Between E8 and E12, the mesenchymal area of each region remained surprisingly constant (Fig. 5 B). However, there was a dramatic increase in small intestinal length (17.6 mm at E8 to 71.1 mm at E12) over the same time period. Indeed, between E6 and E12, the small intestine roughly doubled in length every two days elongating at an average rate of 11 mm/day (Fig. 5 C).

Between E12 and E16, there was a notable increase in cross-sectional area throughout all four regions of the small intestine (Fig. 5 B). There was also an increase in small intestinal length over these stages. The rate of intestinal lengthening between E6 and E16 was relatively steady averaging close to 10 mm/day (Figure 5C, black line). However, this steady rate of growth represented a 4-fold increase in length between E8 and E12 and only a 1.5-fold increase between E12 and E16 (Figure 5C, gray line). Thus, the rapid increase in mesenchymal cross-sectional area at E12 correlates with a decrease in the relative change in length.

Development of the muscularis layers and myofibroblasts

We next examined differentiation of the mesenchymal compartment. While initially uniform in appearance, the mature mesenchymal compartment is composed of varied tissue types including multiple layers of visceral smooth muscle that provide the force for peristaltic contractions. Other mesenchymal cells with limited contractile ability include the subepithelial myofibroblasts that closely surround the crypts and line the mucosa into the villi. Using studies of the chicken as a reference, we expected four layers of visceral smooth muscle to develop in the quail small intestine: inner longitudinal, inner circular, outer circular, and outer longitudinal (Gabella, 1985; Gabella, 2002). These layers are largely distinguished based on morphological features; however, the outer circular layer of the adult

chicken can also be identified molecularly as α-smooth muscle actin (α-SMA) expression is almost entirely replaced by γ-smooth muscle actin (γ-SMA) expression (Gabella, 1985; Yamamoto, 1996).

We utilized immunofluorescence for α- and γ-SMA to generate a comprehensive timeline of visceral smooth muscle and myofibroblast development in the quail small intestine. Faint staining for both α- and γ-SMA was first observed at E6 in a rudimentary circular layer (OC) within the mesenchyme. SMA-negative mesenchymal cells were found on both the luminal and coelomic aspects (Fig. 6 A–D, asterisks). At E10, an α-SMA-positive, γ-SMA-negative outer longitudinal (OL) layer was first observed within the submesothelial region (Fig. 6 E–H). The inner circular (IC) layer was first distinguishable at E14 due to high levels of α-SMA and low levels of γ-SMA at the innermost aspect of the circular muscle layer (Fig. 6 I–L). Also at E14, α-SMA-positive cells could occasionally be identified within the villi (data not shown). At E16, an α- and γ-SMA-positive inner longitudinal layer (IL) was visible and robust α-SMA-positive staining was present within the villi. The submucosal mesenchyme was concurrently reduced to a thin layer (asterisk) and the outer circular layer exhibited decreased staining for α-SMA (Fig. 6 M–P). Finally, in the adult small intestine, γ-SMA was identified in all four layers of visceral smooth muscle but the outer circular layer did not stain for α-SMA at appreciable levels. Additionally, the intestinal crypts were directly adjacent to the inner longitudinal visceral smooth muscle layer without any intervening submucosal mesenchyme (Fig. 6 Q–T, arrows). Thus, the structure of the adult quail small intestine is similar to other avians, including the chicken (Gabella, 1985). The current study demonstrates that contractile cell differentiation in the quail intestine occurs in the following progression: outer circular layer at E6, outer longitudinal layer at E10, inner circular layer at E14, and inner longitudinal layer and subepithelial myofibroblasts at E16.

The organization of the endothelial plexus

Elaboration of the vasculature is critical for organ formation. The vasculature of the intestine is housed within the mesenchymal layer. The major arteries supplying the intestine (mesenteric arteries) branch from the aorta and reach the intestine by means of a mesentery (two mesothelial membranes closely apposed to one another). Once the mesenteric arteries reach the intestine, the large, muscularized branches stay near the surface subjacent to the thin outer longitudinal layer of visceral smooth muscle. Other branches dive deep to supply a second tier of blood vessels that resides near the junction of the lamina propria and inner longitudinal smooth muscle layer. The third and most expansive tier is the extensive capillary network extending into the villi and localized just below the mucosal epithelium (Powell et al., 2011). The initial arrangement of the intestinal primordium with both basement membranes within microns of one another (at E2.1, (Meier, 1980)) allows a single, central endothelial plexus to contact both basement membranes and epithelia. The expansion of the mesenchyme necessitates growth and remodeling of the vascular plexus for this relationship to be maintained.

To understand how the vasculature of the intestine is remodeled from a single centrally located endothelial plexus into a multi-tiered vascular network, we utilized QH1 (quail endothelial cell marker) staining and Tg(*tie1*:H2B-eYFP) quail embryos. These transgenic embryos express an H2B-eYFP fusion protein under control of the endothelial specific *Tie1* promoter (Poynter and Lansford, 2008; Sato et al., 2010). At E2.1 (HH14), endothelial cells were in close approximation to both the endoderm and splanchnic mesoderm (Fig. 7 A–B, arrowheads). At E3 (HH18), eYFP-positive endothelial cells were distributed along the medial-lateral axis of the intestinal primordium but remained within the middle of the mesenchymal layer thus losing close contact with both the endodermal and outer epithelial basement membranes (Fig. 7 C–D, arrowheads). This configuration was maintained until E6 at which time the eYFP-positive cells were organized into two layers one subjacent to the

mesothelium and another layer juxtaposed to the developing submucosal layer (Fig. 7 E–F, arrowheads). The two tiered endothelial network visible at E6 was also reported in Nagy et al. (2009).

At E10, the external endothelial layer was localized below the newly differentiated outer longitudinal visceral smooth muscle cell layer thus occupying the same space where the major vessels will be found in the adult. At this stage, villi were also first observed in the anterior region of the small intestine (Fig. 8 A–F) though the posterior region only had small ridges protruding into the lumen (Fig. 8 G–L). Notably, endothelial cells of the internal plexus (arrowheads) throughout both the anterior and posterior small intestine did not extend into the villi or ridges (Fig. 8 A–L). We first observed endothelial cells within the villi at E14 in low numbers, four days after villi were apparent in the anterior portion of the gut tube (Fig. 9 A–C, arrowheads). By E16, endothelial cells were found in abundance within the villi (Fig. 9 D–F, arrowheads). Cells within the outer endothelial tier became fewer in number over time (Fig. 9 C, F, arrows). Thus, development of the enteric endothelial network progresses through four phases. First, endothelial cells are scattered throughout the mesenchymal space. Second, they organize into two layers in the submesothelial region and submucosal mesenchyme, respectively. Third, differentiation of the outer longitudinal smooth muscle leads to localization of the external plexus below the muscle layer. Finally, endothelial cells penetrate the lamina propria of the villi.

Generation of muscularized surface blood vessels

While the vasculature of the villi remains as a capillary plexus, the vessels near the surface of the adult intestine are large caliber and muscularized. We next examined Tg(*tie1*:H2B-eYFP) intestines in whole mount to determine when large surface blood vessels were formed. At E6, the stage at which two distinct layers of endothelial cells were first apparent within the gut wall, there were not any major surface vessels (Fig. 10 A–B). Instead, endothelial cells were uniformly distributed in a honeycomb-like pattern (Fig. 10 B). By E10, mesenteric branches extending to the intestine were observed (arrows) though there were still no large vessels visible on the intestine proper (Fig. 10 C–D). At E11, we first observed large blood vessels extending from the dorsal mesentery over the gut tube proper (Fig. 10 E–F, arrowheads). Throughout subsequent stages, the major vessels elongated to encompass a greater portion of the intestinal circumference (E12, E13; Fig. 10 G–J, arrowheads).

A further mark of blood vessel maturity is recruitment and differentiation of vascular smooth muscle cells. We used immunofluorescence for α-SMA to determine when cells of the intestinal vasculature were muscularized. At E12, α-SMA staining was present within the outer longitudinal and outer circular smooth muscle layers but was not identified surrounding the eYFP-positive endothelial cells (Fig. 11 A–B). At E14, a single layer of α-SMA-positive cells surrounded the large blood vessels found near the surface of the intestine (Fig. 11 C–D, arrowheads). At E16, rare blood vessels were observed containing multiple layers of vascular smooth muscle cells (Figure 11 E–F, arrowheads). In the adult intestine, large arteries with multiple layers of vascular smooth muscle were readily identified (Figure 11 G–H, arrowheads). Neighboring veins were large caliber though still poorly muscularized (Figure 11 G–H, arrows). Additionally, the second tier of blood vessels near the base of the villi were muscularized in the adult only (Figure 11 G, yellow arrowhead). Thus, the major blood vessels of the intestine are not muscularized until near hatching.

Discussion

Splanchnic mesoderm generates the bulk of the intestine and will diversify into serosa, connective tissue, musculature, and the enteric vasculature. However, relatively little is

known about the development of the intestinal mesoderm. Our study provides a comprehensive examination of the major morphological changes that occur within the intestinal mesoderm starting with the establishment of the intestinal primordium and ending with the definitive structure. Through concurrent examination of multiple features, we were able to identify temporal and spatial coordination between previously unlinked developmental events (Table 1). An examination of four critical time periods in intestinal mesoderm development is presented below highlighting novel correlations illustrated by this study. These data provide developmental biologists and clinicians with a detailed baseline of normal development—the context with which perturbations of intestinal development generated by experimental manipulation and disease can be evaluated. Finally, this comprehensive analysis reveals heretofore unidentified cell and tissue relationships that generate numerous questions for future study.

Appearance of the intestinal anlage

Although not immediately apparent, the eventual architecture of the mature intestine is in fact represented in three features of the intestinal primordium. At the most fundamental level, the endoderm is localized ventrally and the mesoderm, dorsally in the flat intestinal anlage. Thus, when a tube is formed by folding the flat sheet ventrally, the endoderm will line the lumen and the mesoderm will form the coelomic surface reflecting their position in the adult structure. Second, the primordium is split into three compartments by two basement membranes, an arrangement maintained into maturity. Finally, from its earliest appearance, the vascular plexus is localized in the mesenchymal compartment juxtaposed to both basement membranes (Meier, 1980). These basic elements form the structural scaffold around which the flat sheet of the primordium folds to form a tube. Within this context, the mesenchymal space and its resident cells expand to generate the largest intestinal compartment, and the vasculature matures into a multi-tiered network.

Development of the mesenchymal compartment: E1.9–E5

Starting from this basic structure, the first significant change in intestinal mesoderm development is the generation of a multi-layered mesenchyme. Though forming the bulk of the intestine in the adult, this layer is essentially absent in the primordium—the endothelial plexus of the intestine is the only cell population to reside in the mesenchymal compartment and contacts the basement membranes of both the endoderm and splanchnic mesoderm. The rapid cellular expansion of the mesenchymal compartment between E2.2 and E3.5 occurred concurrently with a breakdown of the outer basement membrane likely due to an ingress of cells from the outer epithelium into the mesenchyme. At E3.5, the mesenchymal compartment peaked in width and the outer epithelial basement membrane returned to an unbroken configuration. Throughout the subsequent stages in which a solid basement membrane was present the width of the mesenchymal compartment gradually decreased. A slight increase in mesenchymal width was observed at E5, which correlated with a second brief breakdown of the outer epithelial basement membrane. These features suggest the following sequence: inward migration of cells from the outer epithelium into the mesenchyme, cessation of migration and repair of the basement membrane, a second wave of inward migration, and final repair of the basement membrane. The potential of two temporally separated waves of migration into the mesenchymal space may indicate that specific mesenchymal lineages are added sequentially as suggested but not conclusively proven by cell lineage tracing studies (Wilm et al., 2005; Winters et al., 2012).

Completion of intestinal tube formation: E5–E6

The next major change in intestinal development is the completion of tube formation that occurs at E6. At this stage, the mesothelium is fully differentiated, SMA is first observed in

the outer circular visceral smooth muscle layer and the endothelial plexus splits into two layers. Each of these topics is considered below.

Mesothelial differentiation in the intestine has only recently been studied in any detail (Wilm et al., 2005; Kawaguchi et al., 2007; Winters et al., 2012). In contrast, mesothelial development in the heart has been examined extensively. Cardiac mesothelium is derived from a localized, extrinsic progenitor pool that migrates to the heart. Once at the surface of the heart, individual mesothelial cells undergo an epithelial-mesenchymal transition (EMT) to invade the underlying myocardium and give rise to vascular smooth muscle cells and intracardiac fibroblasts (Mikawa and Gourdie, 1996; Dettman et al., 1998; Männer, 1999; Pérez-Pomares et al., 2002; Guadix et al., 2006). Mesothelial cells of the intestine have a similar potential demonstrated by genetic lineage tracing in the mouse but are derived from a broadly distributed progenitor population intrinsic to the forming gut tube (Wilm et al., 2005). The second brief breakdown of the outer basement membrane of the intestine occurred as the outer epithelium differentiated into a mesothelial layer. Thus, the second wave of inward migration into the mesenchyme may be specific to mesothelial cells or their progenitors providing cells of the future vascular or fibroblast lineage. The molecular regulation of EMT of the cardiac mesothelium has been investigated utilizing multiple murine genetic models (Wu et al., 2010; Baek and Tallquist, 2012). It may be of interest to examine these genetic models in the context of intestinal development to determine if a similar molecular network regulates EMT of mesothelia in the two organs.

In addition to contributing cells, mesothelium is also a signaling center during development (White, 2006; Olivey and Svensson, 2010; Svensson, 2010). The first visceral smooth muscle layer of the intestine differentiates in close proximity to the mesothelium with only a small layer of intervening SMA-negative cells. Endodermal Shh signals are known to be repressive to visceral smooth muscle differentiation in the chick thus positioning the initial layer at a distance from the mucosa (Sukegawa et al., 2000; Gabella, 2002). However, both *Shh* and *Ihh* knockouts in the mouse led to reduced visceral smooth muscle differentiation suggesting the role of Shh is not repressive alone (Ramalho-Santos et al., 2000; Mao et al., 2010). Intestinal mesothelial signaling has not been investigated though frequently, developmental patterning is the result of integration of signals from two opposing sources (Irish et al., 1989; Meinhardt, 2009). Precise positioning of the initial circular muscle layer and subsequent layers of smooth muscle may be the result of both endodermal and mesothelial signaling events though further investigation is required.

The endothelial plexus also divides into two layers at E6 (Nagy et al., 2009). Signals that pattern the intestinal vasculature are currently unknown. As cells are added to the mesenchyme, the endothelial plexus remains centrally located with increasing distance separating it from both basement membranes; thus, hypoxia might be proposed as a potential regulatory signal. However, quantification of the width of the mesenchymal compartment revealed there is actually a decrease in the distance separating the two basement membranes between E3.5 and E6. Thus, division of the endothelial plexus into two layers at this time may not be related simply to increased hypoxia due to mesenchymal growth. The division into two layers that reside near the mesothelial and mucosal surface, respectively, suggests chemotactic cues may originate from both epithelia to produce this pattern though further research is needed in this area.

Maturation of visceral smooth muscle and vascular components: E6–E16

The next major changes that occur within the mesenchymal compartment include differentiation of the remaining visceral smooth muscle cell layers, vascular remodeling and maturation, and extensive growth. It is unknown what directs the sequential differentiation of individual visceral smooth muscle cell layers though, as described above, roles for both

the endoderm and mesothelium are possible. Interestingly, the appearance of the villi is temporally associated with generation of the outer circular and outer longitudinal visceral smooth muscle cell layers suggesting a potential mechanical relationship.

In studies of murine intestinal development, endothelial cells appear to play an important role in villus formation and remain in close association with the endoderm throughout (Hashimoto et al., 1999; Kim et al., 2007). In the quail, villi form independent of a close morphological relationship with the vasculature. Indeed, endothelial cells do not invade the villi until days after they are formed. The cues leading to endothelial ingrowth into the villi are unknown. Also of potential interest, subepithelial myofibroblasts differentiate concurrent with endothelial migration into villi. Endothelial cells in endodermally-derived organs function in paracrine signaling independent of their function in supplying vascular flow to an area (Lammert et al., 2001; Matsumoto et al., 2001; Yoshitomi and Zaret, 2004; Jacquemin et al., 2006). Thus, regulation of villus maturation and myofibroblast differentiation may be related to signaling events from the nearby endothelial cells.

Finally, while the endothelial plexus of the intestinal primordium is thought to be derived from the splanchnic mesoderm (Meier, 1980; Pardanaud et al., 1989; Drake et al., 1997), the origin of the large surface blood vessels is unclear. They are first visible in the mesentery and subsequently over the intestine suggesting they may grow via angiogenesis from the vitelline artery. Alternatively, they may be derived completely from remodeling of the existing endothelial plexus.

As detailed above, there remains much to be understood about intestinal development. Knowledge of the morphological underpinnings is vital if investigations of intestinal formation are to be placed into the larger context in which they occur. These studies provide a timeline of intestinal mesodermal development integrating information about multiple foundational features. With a broad view of intestinal development, potential interactions can be identified that range from the level of gene function, through cellular interactions, to tissue morphogenesis leading to the establishment of the definitive structure.

Experimental Procedures

Embryos

Quail embryos (*Coturnix coturnix japonicia*) were obtained from Ozark Egg Farm (Stover, Missouri). Tg(*tie1*:H2B-eYFP) quail embryos were a generous gift from Dr. Rusty Lansford (Caltech, Pasadena, CA). All eggs were incubated at 37°C in humidity and staged according to the Japanese quail and the Hamburger Hamilton staging chart (Hamburger and Hamilton, 1992; Ainsworth et al., 2010). Adult intestines were isolated from mature four-month-old wild type quail.

Immunofluorescence

All embryos and tissue were fixed in 4% formaldehyde (Sigma F1635) in PBS (pH 7.4) at room temperature or 4°C depending on tissue size. The samples were washed with PBS (pH 7.4), cryoprotected in 30% sucrose, embedded in OCT (TissueTek 4583) and transversely sectioned (unless otherwise noted) at 5μm. Sections were rehydrated, washed with PBS, and permeabilized with 0.2% Triton-X 100 (Sigma T9284) in PBS for ten minutes, washed with PBS, and blocked in 10% goat serum (Invitrogen 16210-072) + 1% BSA (Sigma A2153) in PBS. Samples were then treated with primary antibodies (see below) overnight at 4°C. Slides were then washed with PBS and incubated with secondary antibodies (see below) for 60 min. at room temperature. Slides were washed and mounted with ProLong Gold mounting agent (Invitrogen P36930).

Antibodies

Primary antibodies: laminin (Abcam ab11575; 1:200), cytokeratin (Abcam ab9377; 1:200), laminin (DSHB, 3H11 and 31 or 31-1; 1:25 (each)), anti-GFP (Invitrogen, A11122; 1:200), anti-αSMA Clone 1A4 (Sigma A2547; 1:200), αSMA (Abcam ab5694; 1:200), γSMA (MP Biomedicals 69133; 1:600). Secondaries: Alexa 488 and 568 (Invitrogen A11001, A11004; 1:500), TOPRO-3 (Invitrogen T3605; 1:1000), DAPI (Invitrogen D3571; 1:10,000).

Microscopy

Immunofluorescence was imaged using an Olympus Fluo-View1000 confocal microscope (Vanderbilt CISR Core). Images were taken in Z-stack format and analyzed using FV-1000, Metamorph and Photoshop software. Images in Figure 7 A–B were taken in Z-stack format on a Zeiss LSM 510 confocal microscope and analyzed in the LSM software. Brightness and contrast of all images were adjusted for visual representation in Photoshop.

Morphometric Analysis

Small intestine sections were stained with laminin antibody and imaged on an EVOS microscope (Joe Roland, Goldenring Lab, Vanderbilt). ImageJ software was used to measure the distance between the outer and endodermal basement membranes of intestines aged E1.9 through E6 (eight to twenty samples analyzed at each stage). The distances were averaged and the standard deviation and standard error of the mean were calculated in Excel. To determine the area of the mesenchymal space, six to ten samples were analyzed for each intestinal region (posterior, middle posterior, middle anterior, anterior) of each intestinal stage including: E8, E10, E12, E14, E16. Metamorph software (Vanderbilt CISR) was utilized to specify the mesenchymal region (area between outer and endodermal basement membranes). Average, standard deviation, and standard error of mean were calculated in Excel. To determine the total length of the intestines, samples were dissected from quail embryos and the mesentery and vessels completely removed. Four to ten samples were measured for each stage including E6, E8, E10, E12, E14, E16. Averages, standard deviation, and standard error of mean were calculated in Excel.

Acknowledgments

Imaging was performed in part through the use of the VUMC Cell Imaging Shared Resource (supported by NIH grants CA68485, DK20593, DK58404, HD15052, DK59637 and EY08126). Monoclonal antibodies were ordered from the Developmental Studies Hybridoma Bank developed under the support of the NICHD and maintained by The University of Iowa, Department of Biology, Iowa City, IA 52242. We thankfully acknowledge Dr. Rusty Lansford and David Huss (CalTech) for supplying Tg(*tie1*:H2B-eYFP) quail eggs and adult intestines for analysis. We also acknowledge Sean Schaffer (VUMC CISR) for his assistance with the morphometric calculations in Metamorph.

Grant Sponsor: National Institutes of Health grant R01 DK83234 and National Institutes of Health grant P30 DK058404

References

Ainsworth SJ, Stanley RL, Evans DJR. Developmental stages of the Japanese quail. J Anat. 2010; 216:3–15. [PubMed: 19929907]

Appelman HD. Morphology of gastrointestinal stromal tumors: Historical perspectives. J Surg Oncol. 2011; 104:874–881. [PubMed: 22069172]

Baek ST, Tallquist MD. Nf1 limits epicardial derivative expansion by regulating epithelial to mesenchymal transition and proliferation. Development. 2012; 139:2040–2049. [PubMed: 22535408]

Burns AJ, Roberts RR, Bornstein JC, Young HM. Development of the enteric nervous system and its role in intestinal motility during fetal and early postnatal stages. Semin Pediatr Surg. 2009; 18:196–205. [PubMed: 19782301]

Coulombre AJ, Coulombre JL. Intestinal developmentIMorphogenesis of the villi and musculature. J Embryol Exp Morphol. 1958; 6:403–411. [PubMed: 13575653]

Dauça M, Bouziges F, Colin S, Kedinger M, Keller MK, Schilt J, Simon-Assmann P, Haffen K. Development of the vertebrate small intestine and mechanisms of cell differentiation. Int J Dev Biol. 2007; 34:205–218.

Dettman RW, Denetclaw W, Ordahl CP, Bristow J. Common epicardial origin of coronary vascular smooth muscle, perivascular fibroblasts, and intermyocardial fibroblasts in the avian heart. Dev Biol. 1998; 193:169–181. [PubMed: 9473322]

Drake CJ, Brandt SJ, Trusk TC, Little CD. TAL1/SCL is expressed in endothelial progenitor cells/angioblasts and defines a dorsal-to-ventral gradient of vasculogenesis. Dev Biol. 1997; 192:17–30. [PubMed: 9405094]

Eddinger TJ. Unique contractile and structural protein expression in dog ileal inner circular smooth muscle. J Smooth Muscle Res. 2009; 45:217–230. [PubMed: 19907120]

Gabella G. Structure of the musculature of the chicken small intestine. Anat Embryol (Berl). 1985; 171:139–149. [PubMed: 3985363]

Gabella G. Development of visceral smooth muscle. Results Probl Cell Differ. 2002; 38:1–37. [PubMed: 12132390]

Grey RD. Morphogenesis of intestinal villiIScanning electron microscopy of the duodenal epithelium of the developing chick embryo. J Morphol. 1972; 137:193–213. [PubMed: 4555575]

Grosse AS, Pressprich MF, Curley LB, Hamilton KL, Margolis B, Hildebrand JD, Gumucio DL. Cell dynamics in fetal intestinal epithelium: implications for intestinal growth and morphogenesis. Development. 2011; 138:4423–4432. [PubMed: 21880782]

Guadix JA, Carmona R, Muñoz-Chápuli R, Pérez-Pomares JM. In vivo and in vitro analysis of the vasculogenic potential of avian proepicardial and epicardial cells. Dev Dyn. 2006; 235:1014–1026. [PubMed: 16456846]

Guzman MA, Prasad R, Duke DS, de Chadarévian J-P. Multiple intestinal atresias associated with angiodysplasia in a newborn. J Pediatr Surg. 2011; 46:1445–1448. [PubMed: 21763851]

Hamburger V, Hamilton HL. A series of normal stages in the development of the chick embryo 1951. Dev Dyn. 1992; 195:231–272. [PubMed: 1304821]

Hashimoto H, Ishikawa H, Kusakabe M. Development of vascular networks during the morphogenesis of intestinal villi in the fetal mouse. Kaibogaku zasshi. J Anat. 1999; 74:567–576.

Heanue TA, Pachnis V. Enteric nervous system development and Hirschsprung disease: advances in genetic and stem cell studies. Nat Rev Neurosci. 2007; 8:466–479. [PubMed: 17514199]

Hiramatsu H, Yasugi S. Molecular analysis of the determination of developmental fate in the small intestinal epithelium in the chicken embryo. Int J Dev Biol. 2004; 48:1141–1148. [PubMed: 15602700]

Hirota S, Isozaki K, Y M, Hashimoto K, Nishida T, Ishiguro S, Kawano K, Hanada M, Kurata A, Takeda M, Muhammad Tunio G, Matsuzawa Y, Kanakura Y, Shinomura Y, Kitamura Y. Gain-of-function mutations of c-kit in human gastrointestinal stromal tumors. Science. 1998; 279:577–580. [PubMed: 9438854]

Huss D, Poynter G, Lansford R. Japanese quail (Coturnix japonica) as a laboratory animal model. Lab Anim (NY). 2008; 37:513–519. [PubMed: 18948991]

Irish V, Lehmann R, Akam M. The Drosophila posterior-group gene nanos functions by repressing hunchback activity. Nature. 1989; 338:646–648. [PubMed: 2704419]

Jacobson LF, Noer RJ. The vascular pattern of the intestinal villi in various laboratory animals and man. Anat Rec. 1952; 114:85–101. [PubMed: 12986266]

Jacquemin P, Yoshitomi H, Kashima Y, Rousseau GG, Lemaigre FP, Zaret KS. An endothelial-mesenchymal relay pathway regulates early phases of pancreas development. Dev Biol. 2006; 290:189–199. [PubMed: 16386727]

Kawaguchi M, Bader DM, Wilm B. Serosal mesothelium retains vasculogenic potential. Dev Dyn. 2007; 236:2973–2979. [PubMed: 17948313]

Kim KE, Sung H-K, Koh GY. Lymphatic development in mouse small intestine. Dev Dyn. 2007; 236:2020–2025. [PubMed: 17576138]

Lammert E, Cleaver O, Melton D. Induction of pancreatic differentiation by signals from blood vessels. Science. 2001; 294:564–567. [PubMed: 11577200]

Lefebvre O, Sorokin L, Kedinger M, Simon-Assmann P. Developmental expression and cellular origin of the laminin alpha2, alpha4, and alpha5 chains in the intestine. Dev Biol. 1999; 210:135–150. [PubMed: 10364433]

Louw JH, Barnard CN. Congenital intestinal atresia; observations on its origin. Lancet. 1955; 269:1065–1067. [PubMed: 13272331]

Madison BB, Braunstein K, Kuizon E, Portman K, Qiao XT, Gumucio DL. Epithelial hedgehog signals pattern the intestinal crypt-villus axis. Development. 2005; 132:279–289. [PubMed: 15590741]

Männer J. Does the subepicardial mesenchyme contribute myocardioblasts to the myocardium of the chick embryo heart? A quail-chick chimera study tracing the fate of the epicardial primordium. Anat Rec. 1999; 255:212–226. [PubMed: 10359522]

Mao J, Kim B-M, Rajurkar M, Shivdasani RA, McMahon AP. Hedgehog signaling controls mesenchymal growth in the developing mammalian digestive tract. Development. 2010; 137:1721–1729. [PubMed: 20430747]

Matsumoto K, Matsumoto K, Yoshitomi H, Rossant J, Zaret KS. Liver organogenesis promoted by endothelial cells prior to vascular function. Science. 2001; 294:559–563. [PubMed: 11577199]

Mazur MT, Clark HB. Gastric stromal tumors. Reappraisal of histogenesis. Am J Surg Pathol. 1983; 7:507–519. [PubMed: 6625048]

McHugh KM. Molecular analysis of smooth muscle development in the mouse. Dev Dyn. 1995; 204:278–290. [PubMed: 8573719]

Meier S. Development of the chick embryo mesoblast: pronephros, lateral plate, and early vasculature. J Embryol Exp Morphol. 1980; 55:291–306. [PubMed: 7373199]

Meinhardt H. Models for the generation and interpretation of gradients. Cold Spring Harb Perspect Biol. 2009; 1:a001362. [PubMed: 20066097]

Mikawa T, Gourdie RG. Pericardial mesoderm generates a population of coronary smooth muscle cells migrating into the heart along with ingrowth of the epicardial organ. Dev Biol. 1996; 174:221–232. [PubMed: 8631495]

Milgrom-Hoffman M, Harrelson Z, Ferrara N, Zelzer E, Evans SM, Tzahor E. The heart endocardium is derived from vascular endothelial progenitors. Development. 2011; 138:4777–4787. [PubMed: 21989917]

Mitjans M, Barniol G, Ferrer R. Mucosal surface area in chicken small intestine during development. Cell Tissue Res. 1997; 290:71–78. [PubMed: 9377644]

Mutsaers SE. Mesothelial cells: their structure, function and role in serosal repair. Respirology. 2002; 7:171–191. [PubMed: 12153683]

Mutsaers SE. The mesothelial cell. Int J Biochem Cell Biol. 2004; 36:9–16. [PubMed: 14592528]

Nagy N, Mwizerwa O, Yaniv K, Carmel L, Pieretti-Vanmarcke R, Weinstein BM, Goldstein AM. Endothelial cells promote migration and proliferation of enteric neural crest cells via beta1 integrin signaling. Dev Biol. 2009; 330:263–272. [PubMed: 19345201]

Newgreen D, Young HM. Enteric nervous system: Development and developmental disturbances--Part 1. Pediatr Dev Pathol. 2002; 5:224–247. [PubMed: 12007016]

Olivey HE, Svensson EC. Epicardial-myocardial signaling directing coronary vasculogenesis. Circ Res. 2010; 106:818–832. [PubMed: 20299672]

Pardanaud L, Yassine F, Dieterlen-Lievre F. Relationship between vasculogenesis, angiogenesis and haemopoiesis during avian ontogeny. Development. 1989; 105:473–485. [PubMed: 2612361]

Pérez-Pomares J-M, Carmona R, González-Iriarte M, Atencia G, Wessels A, Muñoz-Chápuli R. Origin of coronary endothelial cells from epicardial mesothelium in avian embryos. Int J Dev Biol. 2002; 46:1005–1013. [PubMed: 12533024]

Powell DW, Pinchuk IV, Saada JI, Chen X, Mifflin RC. Mesenchymal cells of the intestinal lamina propria. Annu Rev Physiol. 2011; 73:213–237. [PubMed: 21054163]

Poynter G, Lansford R. Generating transgenic quail using lentiviruses. Methods Cell Biol. 2008; 87:281–293. [PubMed: 18485303]

Ramalho-Santos M, Melton DA, McMahon AP. Hedgehog signals regulate multiple aspects of gastrointestinal development. Development. 2000; 127:2763–2772. [PubMed: 10821773]

Sanders KM. A case for interstitial cells of Cajal as pacemakers and mediators of neurotransmission in the gastrointestinal tract. Gastroenterology. 1996; 111:492–515. [PubMed: 8690216]

Sato Y, Poynter G, Huss D, Filla MB, Czirók A, Rongish BJ, Little CD, Fraser SE, Lansford R. Dynamic analysis of vascular morphogenesis using transgenic quail embryos. PloS one. 2010; 5:e12674. [PubMed: 20856866]

Savin T, Kurpios NA, Shyer AE, Florescu P, Liang H, Mahadevan L, Tabin CJ. On the growth and form of the gut. Nature. 2011; 476:57–62. [PubMed: 21814276]

Simon-Assmann P, Kedinger M, De Arcangelis A, Rousseau V, Simo P. Extracellular matrix components in intestinal development. Experientia. 1995; 51:883–900. [PubMed: 7556570]

Spence B, Lauf R, Shroyer N. Vertebrate intestinal endoderm development. Dev Dyn. 2011; 240:501–520. [PubMed: 21246663]

Streutker CJ, Huizinga JD, Driman DK, Riddell RH. Interstitial cells of Cajal in health and disease. Part I: normal ICC structure and function with associated motility disorders. Histopathology. 2007; 50:176–189. [PubMed: 17222246]

Sukegawa A, Narita T, Kameda T, Saitoh K, Nohno T, Iba H, Yasugi S, Fukuda K. The concentric structure of the developing gut is regulated by Sonic hedgehog derived from endodermal epithelium. Development. 2000; 127:1971–1980. [PubMed: 10751185]

Svensson EC. Deciphering the signals specifying the proepicardium. Circ Res. 2010; 106:1789–1790. [PubMed: 20576940]

Wells JM, Melton DA. Vertebrate endoderm development. Annu Rev Cell Dev Biol. 1999; 15:393–410. [PubMed: 10611967]

White AC. FGF9 and SHH signaling coordinate lung growth and development through regulation of distinct mesenchymal domains. Development. 2006; 133:1507–1517. [PubMed: 16540513]

Wilm B, Ipenberg A, Hastie ND, Burch JBE, Bader DM. The serosal mesothelium is a major source of smooth muscle cells of the gut vasculature. Development. 2005; 132:5317–5328. [PubMed: 16284122]

Winters NI, Thomason RT, Bader DM. Identification of a novel developmental mechanism in the generation of mesothelia. Development. 2012; 139:2926–2934. [PubMed: 22764055]

Wu M, Smith CL, Hall JA, Lee I, Luby-Phelps K, Tallquist MD. Epicardial spindle orientation controls cell entry into the myocardium. Dev Cell. 2010; 19:114–125. [PubMed: 20643355]

Yamamoto Y, Kubota T, Atoji Y, Suzuki Y. Distribution of alpha-vascular smooth muscle actin in the smooth muscle cells of the gastrointestinal tract of the chicken. J Anat. 1996; 189:623. [PubMed: 8982838]

Yoshitomi H, Zaret KS. Endothelial cell interactions initiate dorsal pancreas development by selectively inducing the transcription factor Ptf1a. Development. 2004; 131:807–817. [PubMed: 14736742]

Young H, Bergner A, Anderson R, Enomoto H, Milbrandt J, Newgreen D, Whitington P. Dynamics of neural crest-derived cell migration in the embryonic mouse gut. Dev Biol. 2004; 270:455–473. [PubMed: 15183726]

Young HM, Newgreen D. Enteric neural crest-derived cells: origin, identification, migration, and differentiation. Anat Rec. 2001; 262:1–15. [PubMed: 11146424]

Yung S, Chan TM. Mesothelial cells. Perit Dial Int. 2007; 27(Suppl 2):S110–S115. [PubMed: 17556288]

Zorn AM, Wells JM. Vertebrate endoderm development and organ formation. Annu Rev Cell Dev Biol. 2009; 25:221–251. [PubMed: 19575677]

Key Findings

- A comprehensive description of development of the mesoderm from generation of the primordium into adulthood is presented.
- Intestinal mesoderm development occurs in four major phases: establishment of the primordium, generation of the mesenchyme, closure of the gut tube, maturation of visceral muscle and vasculature.
- Novel spatial and temporal associations are identified throughout each developmental phase.

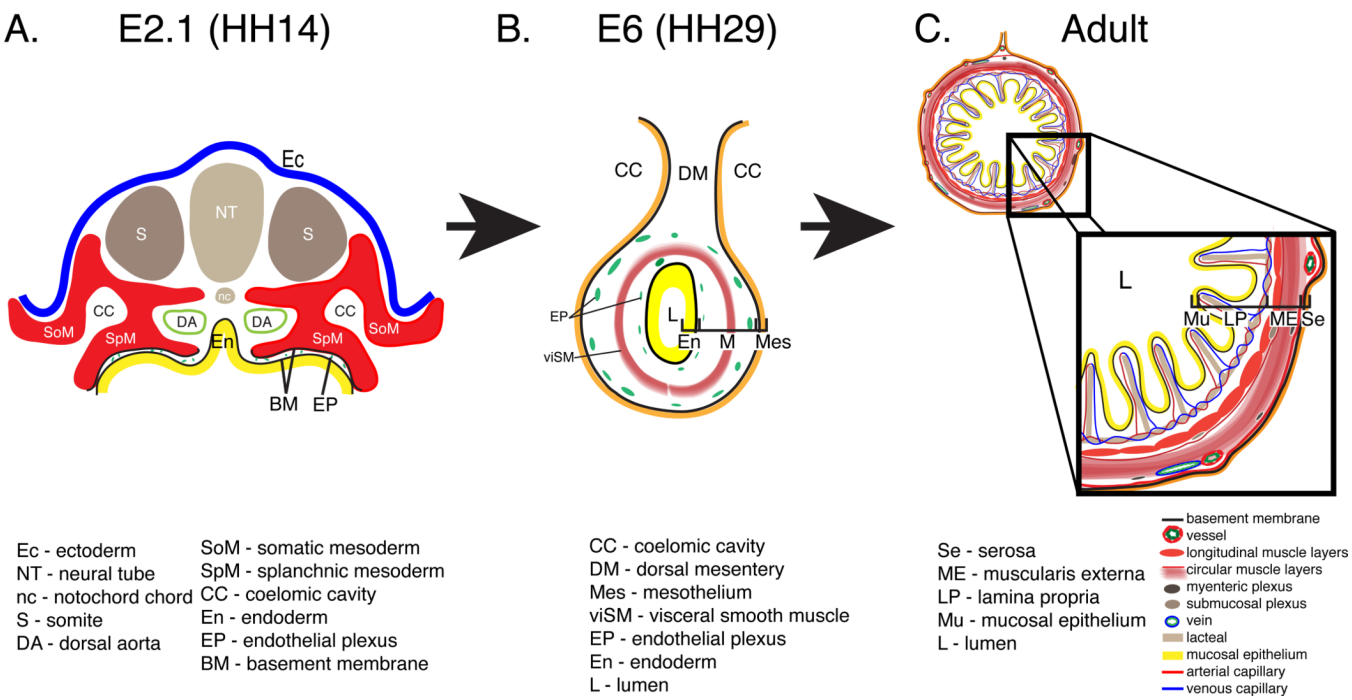

Figure 1. Schematic depicting the intestinal primordium, primitive intestinal tube and adult intestine

A: Transverse section through an embryonic day (E) 2.1 quail embryo equivalent to Hamburger and Hamilton (HH) stage 14. At this stage, the intestinal primordium is open and comprised of the splanchnic mesoderm (red; SpM), endoderm (yellow; En) and an intervening endothelial plexus (green; EP). **B**: At E6, the intestine is completely closed and composed of a mesothelium (orange; Mes), a two layered endothelial plexus (green; EP), a visceral smooth muscle layer (red; viSM), and endoderm (yellow; En). **C**: In the adult intestine, villi are lined with a mucosal epithelium (yellow; Mu) and contain a lamina propria (LP) composed of capillaries, a lymphatic lacteal, and connective tissue. A four-layered muscularis externa (ME) surrounds the lamina propria. A serosal membrane (Se) lines the coelomic surface.

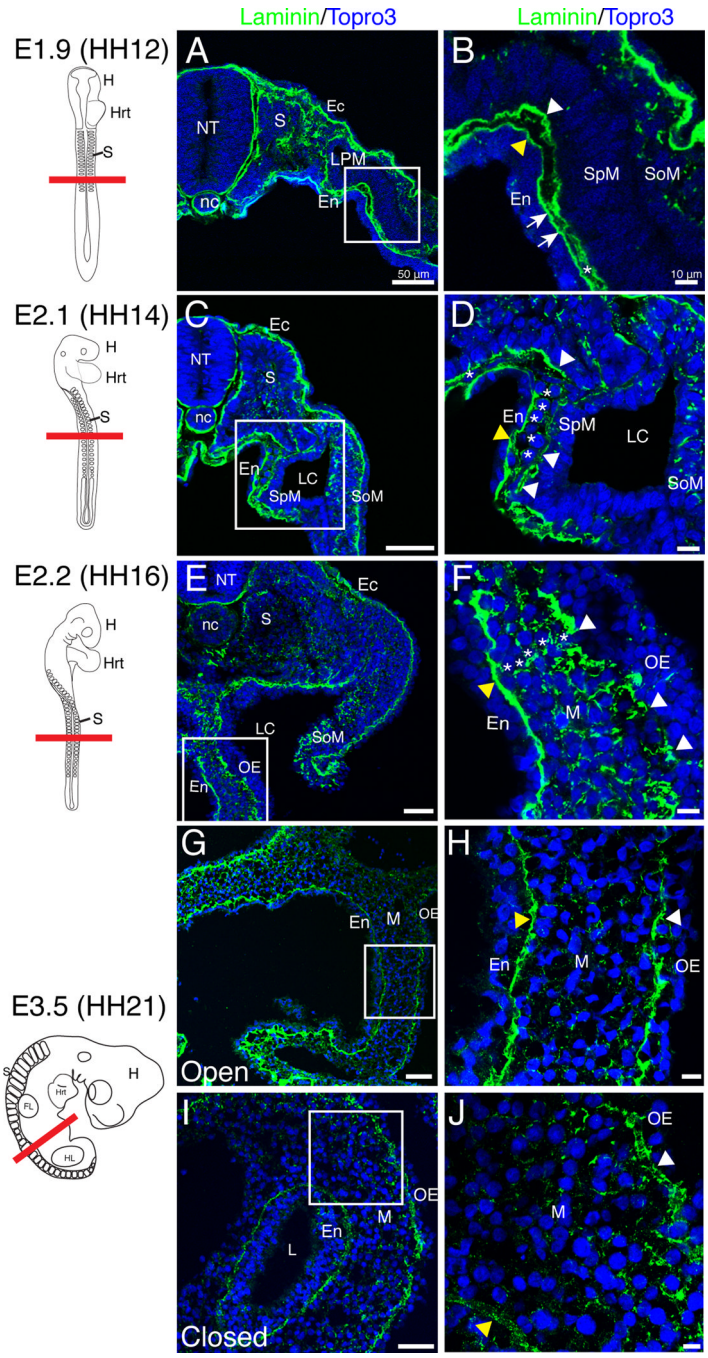

Figure 2. Early basement membrane dynamics in generation of the mesenchymal compartment

Schematics in left column depict quail embryos at the stage isolated and the red line denotes the plane of section. **A–B**: At E1.9, continuous basement membranes (arrowheads) lined the splanchnic mesoderm and endoderm with multiple apparent points of contact (arrows). Asterisk denotes a rare mesenchymal cell. **C–D:** The outer basement membrane (white arrowheads) began to break down at E2.1 and mesenchymal cells were more common (asterisks). The endodermal basement membrane (yellow arrowhead) remained solid. **E–F**: At E2.2, there were multiple mesenchymal cell layers (asterisks) and the outer basement membrane was dispersed (white arrowheads). Yellow arrowhead denotes the endodermal

basement membrane. **G–J**: At E3.5, both the outer epithelial (white arrowhead) and endodermal (yellow arrowhead) basement membranes were continuous in the open and closed intestinal regions. Scale bars: 50μm (A, C, E, G, I) and 10μm (B, D, F, H, J). Ec, ectoderm; En, endoderm; FL, forelimb; H, head; Hrt, heart; HL, hindlimb; L, lumen; LC, lateral cavity; LPM, lateral plate mesoderm; M, mesenchyme; nc, notochord; NT, neural tube; OE, outer epithelium; S, somites; SoM, somatic mesoderm; SpM, splanchnic mesoderm.

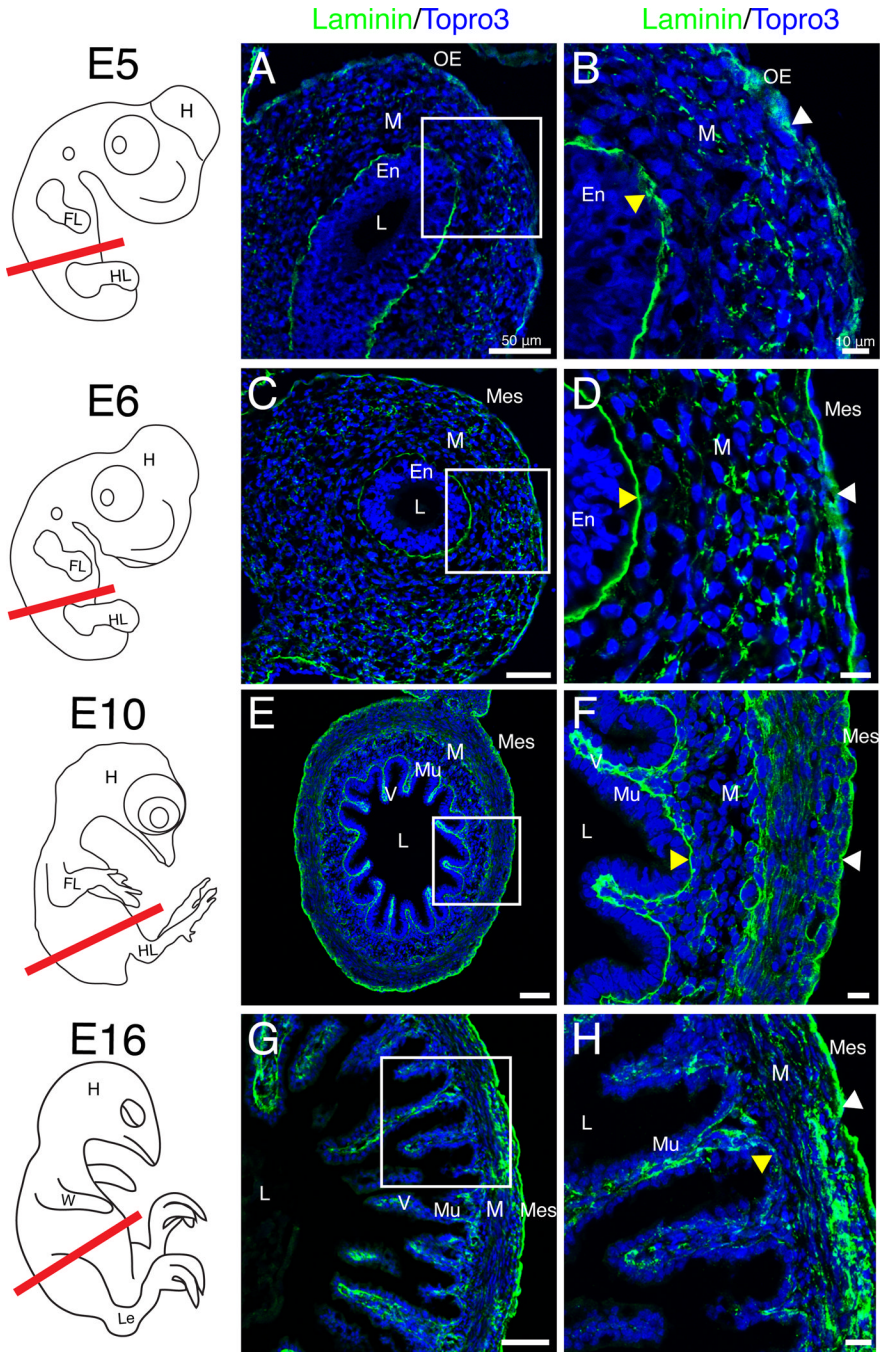

Figure 3. Basement membrane dynamics throughout gut tube closure and mesenchymal differentiation

Schematics in left column depict quail embryos at the stage isolated and the red line denotes the plane of section. **A–B**: At E5, the outer epithelial basement membrane appeared dispersed (white arrowhead). Yellow arrowhead denotes the endodermal basement membrane. **C–D**: At E6, both the outer (white arrowhead) and endodermal (yellow arrowhead) basement membranes were unbroken. **E–F**: At E10, villi (V) were present and both basement membranes were continuous (arrowheads). **G–H**: At E16, the mesenchyme was condensed (compare F and H). The outer basement membrane was robust and unbroken (white arrowhead) while the mucosal basement membrane weakly stained with laminin

(yellow arrowhead). Scale bars: 50μm (A, C, E, G,) and 10μm (B, D, F, H). En, endoderm; FL, forelimb; H, head; HL, hindlimb; L, lumen; Le, leg; M, mesenchyme; Mes, mesothelium; Mu, mucosa; OE, outer epithelium; V, villi; W, wing.

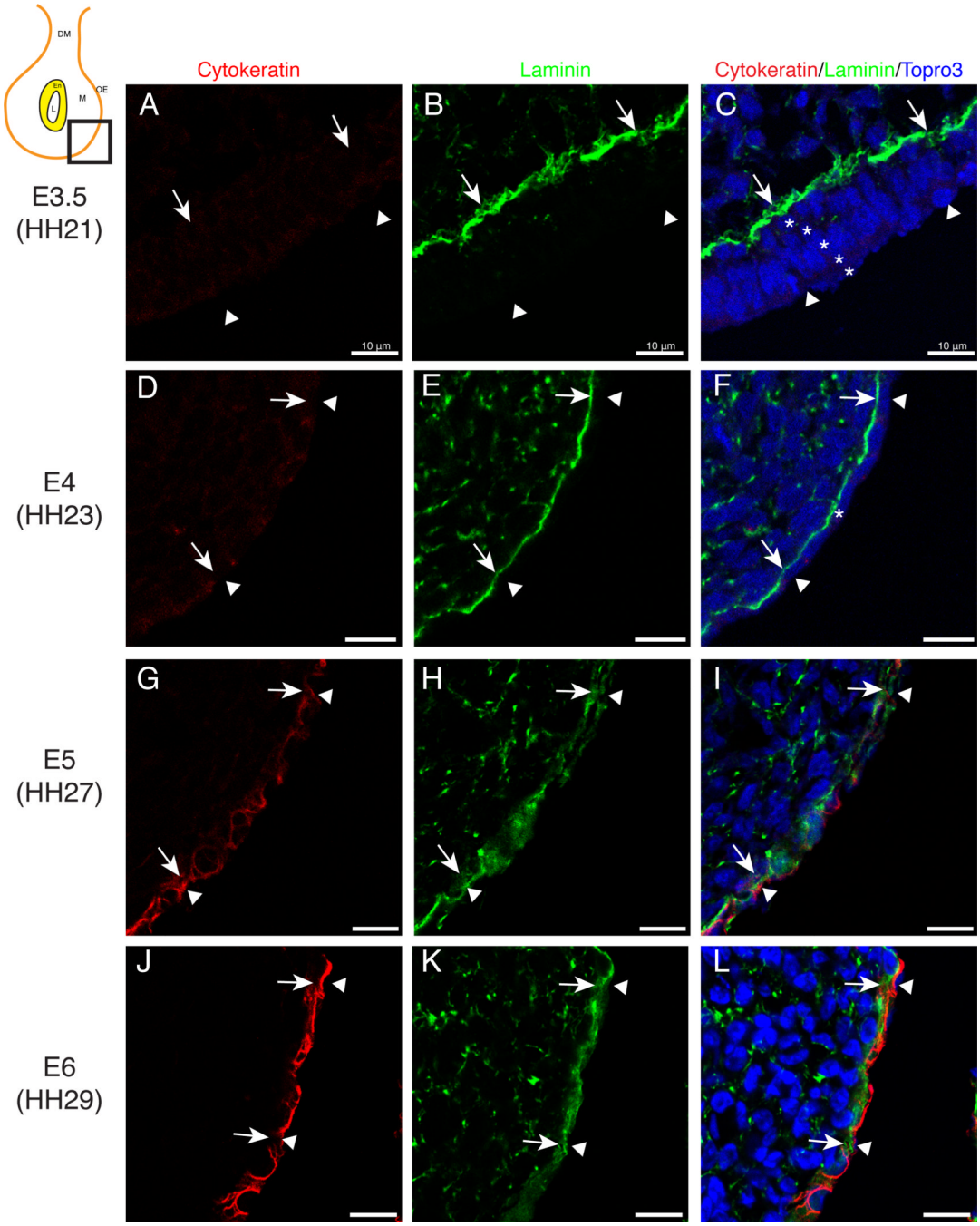

Figure 4. Mesothelial differentiation

Schematic in upper-left corner depicts the region of the gut tube that was imaged. **A–C**: At E3.5, the outer epithelium (arrowheads) was stratified (asterisks) and the basement membrane was continuous (arrows). No cytokeratin staining was evident at this time. **D–F**: At E4, the outer epithelium was a single cell layer thick (arrowheads) with a continuous basement membrane (arrows). Cytokeratin staining was weakly positive. **G–I**: At E5, laminin staining in the outer basement membrane was dispersed (arrows). Cytokeratin staining was present at low levels. **J–L**: At E6, laminin staining (arrows) was unbroken and

cytokeratin staining was robust within the mesothelium (arrowheads). Scale bars: 10μm (A–L). DM, dorsal mesentery; En, endoderm; L, lumen; M, mesenchyme; OE, outer epithelium.

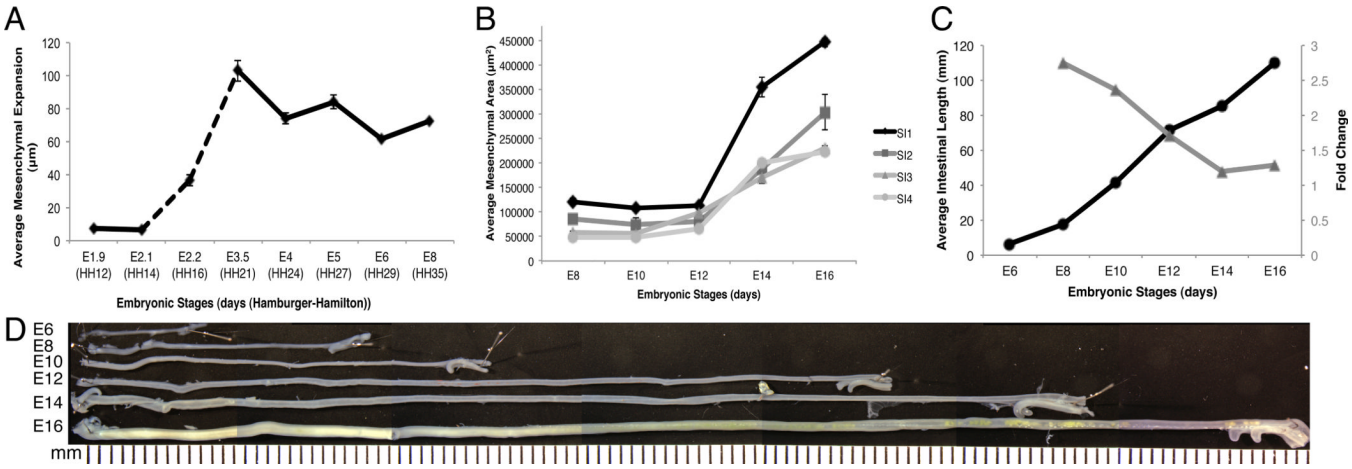

Figure 5. Expansion of the mesenchymal compartment over time

A: Graph of the distance between the outer epithelial and endodermal basement membranes measured at key stages between E1.9 and E8. The dashed line represents the time period over which the outer basement membrane was dispersed. Solid lines indicate a continuous outer basement membrane was present. **B**: Four regions along the anterior-posterior axis of the small intestine (SI 1–4) were analyzed individually for mesenchymal cross-sectional area between E8 and E16. The cross-sectional area of each region was graphed independently. **C**: Small intestinal length measured between E6 and E16 (left y-axis, black circles). Fold change in intestinal length over the same time period (right y-axis, grey triangles). **D**: Photomontage of isolated small intestines with mesentery and blood vessels removed and pinned out to demonstrate their length.

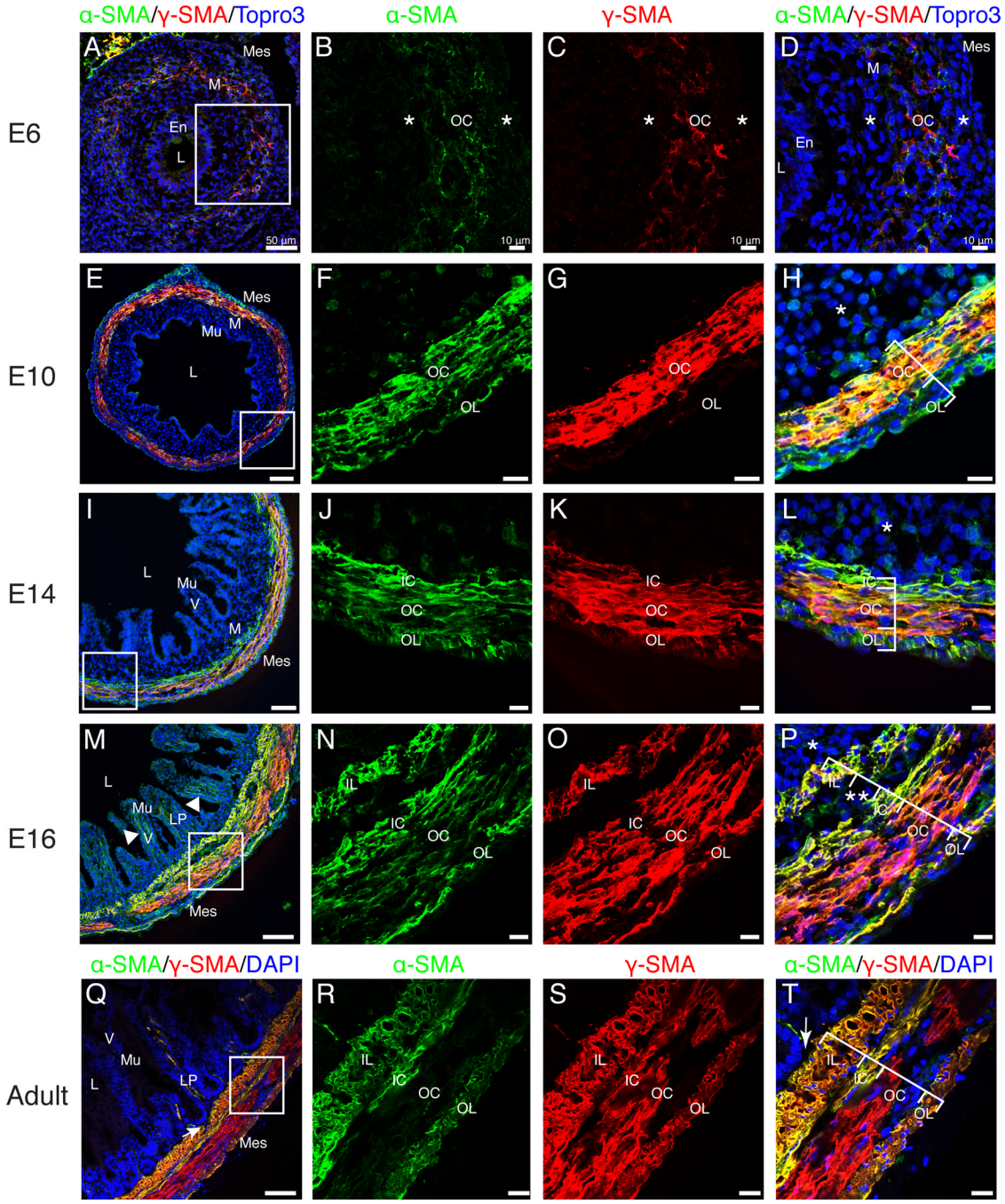

Figure 6. Differentiation of visceral smooth muscle

A–D: At E6, faint staining for α-SMA and γ-SMA defined the outer circular muscle layer. Asterisks represent SMA-negative mesenchymal cells bordering the outer circular muscle layer. **E–H**: Robust staining for α-SMA marked the outer circular and outer longitudinal muscle layers. γ-SMA was observed in the outer circular but not the outer longitudinal layer. SMA-negative submucosal mesenchyme was still present (asterisk). **I–L**: By E14, the inner circular layer (α-SMA-positive, weak γ-SMA) was evident. Asterisk denotes SMA-negative submucosal mesenchyme. **M–P**: At E16, four muscle layers were present including the inner longitudinal layer. All layers stained for both α-SMA and γ-SMA. Double

asterisks denote submucosal neuronal plexus. Limited SMA-negative submucosal mesenchyme was present (asterisk). Arrowhead in M indicates SMA-positive staining within the villi. **Q–T**: In the adult intestine, the four visceral smooth muscle layers were directly subjacent to the lamina propria (arrow) with no intervening submucosal mesenchyme. The outer circular layer was α-SMA-negative. Scale Bars: 50μm (A, E, I, M, Q) and 10μm (B–D, F–H, J–L, N–P, R–T). En, endoderm; IC, inner circular; IL, inner longitudinal; LP, lamina propria; L, lumen; M, mesenchyme; Mes, mesothelium; Mu, mucosa; OC, outer circular; OL, outer longitudinal; V, villi.

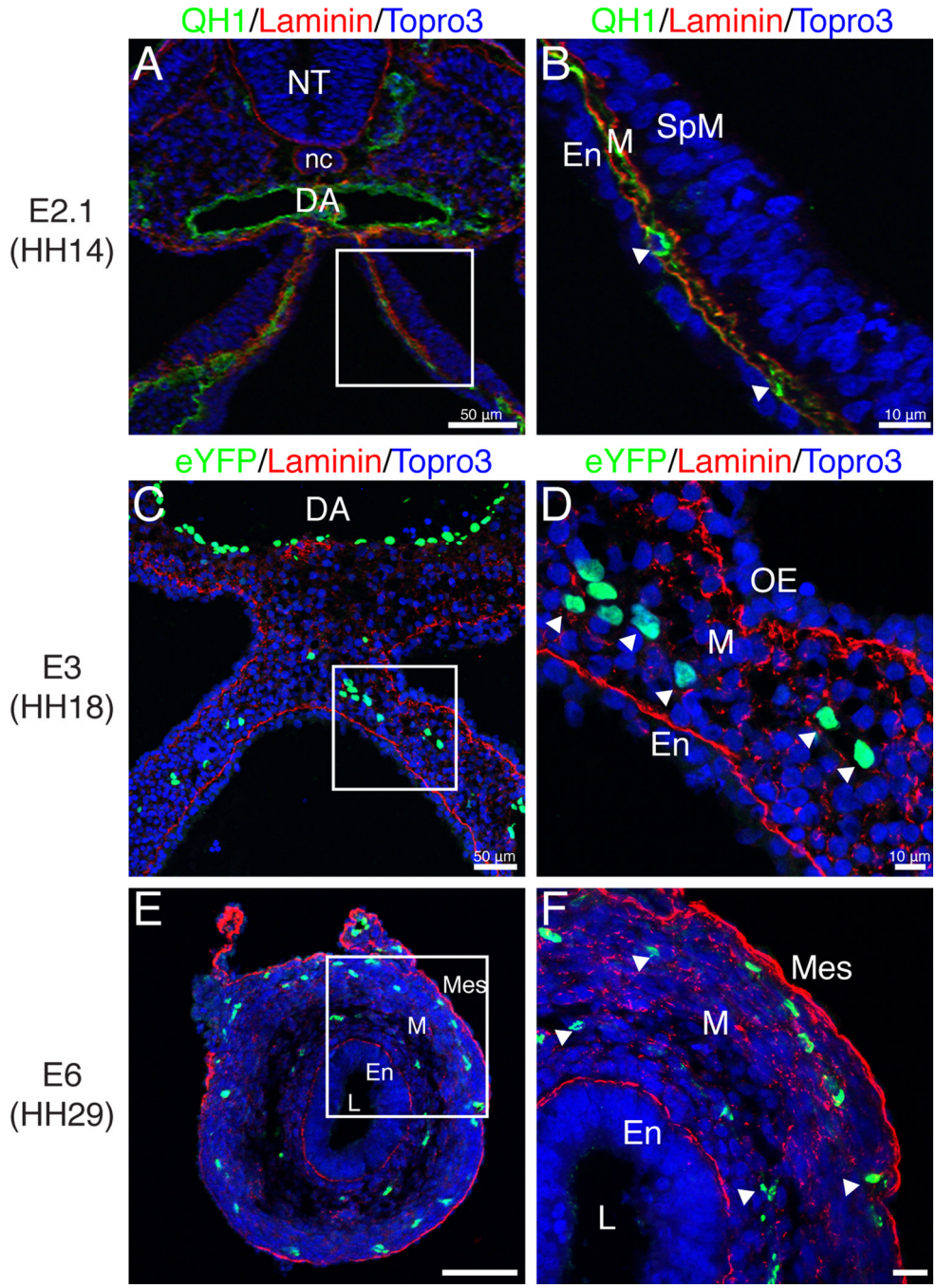

Figure 7. Generation of a two-tiered endothelial plexus

Laminin (basement membrane marker; red), QH1 and eYFP (endothelial markers; green) immunofluorescence. **A–B**: At E2.1, an endothelial plexus marked by QH1 (arrowheads) was present between the endoderm and splanchnic mesoderm. C–F: Sections through Tg(*tie1*:H2B-eYFP) quail intestinal primordia. **C–D**: At E3, the endothelial plexus (arrowheads) was detected in the middle of the multilayered mesenchyme. **E–F**: At E6, the endothelial plexus was organized into two concentric layers below the endoderm and mesothelium, respectively (arrowheads). Scale bars: 50µm (A, C, E) and 10µm (B, D, F).

DA, dorsal aorta; En, endoderm; L, lumen; M, mesenchyme; Mes, mesothelium; nc, notochord; NT, neural tube; OE, outer epithelium; SpM, splanchnic mesoderm.

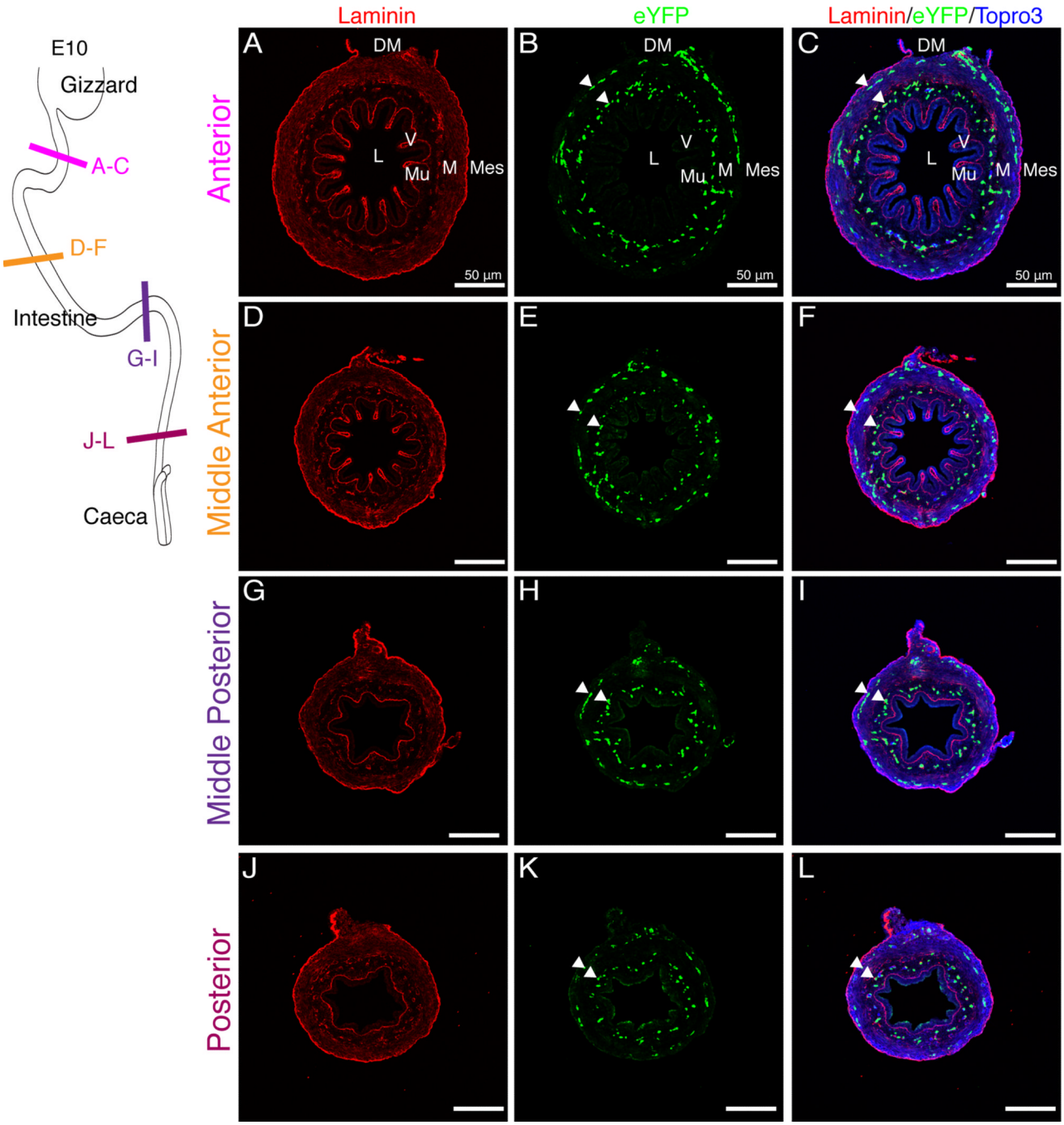

Figure 8. Endothelial plexus remodeling during villi formation

Schematic in upper-left corner depicts the regions of the intestine that were sectioned. E10 intestines were isolated from Tg(*tie1*:H2B-eYFP) embryos. **A–F**: Villi were present in the anterior region of the intestine. The endothelial plexus (eYFP-positive) was organized in two concentric rings (arrowheads) but did not extend into the villi. **G–L**: In the posterior small intestine, ridges but no villi were identified. The endothelial plexus remained organized in two concentric rings (arrowheads). Scale bars: 50µm (A–L). DM, dorsal mesentery; L, lumen; M, mesenchyme; Mes, mesothelium; Mu, mucosa, V, villi.

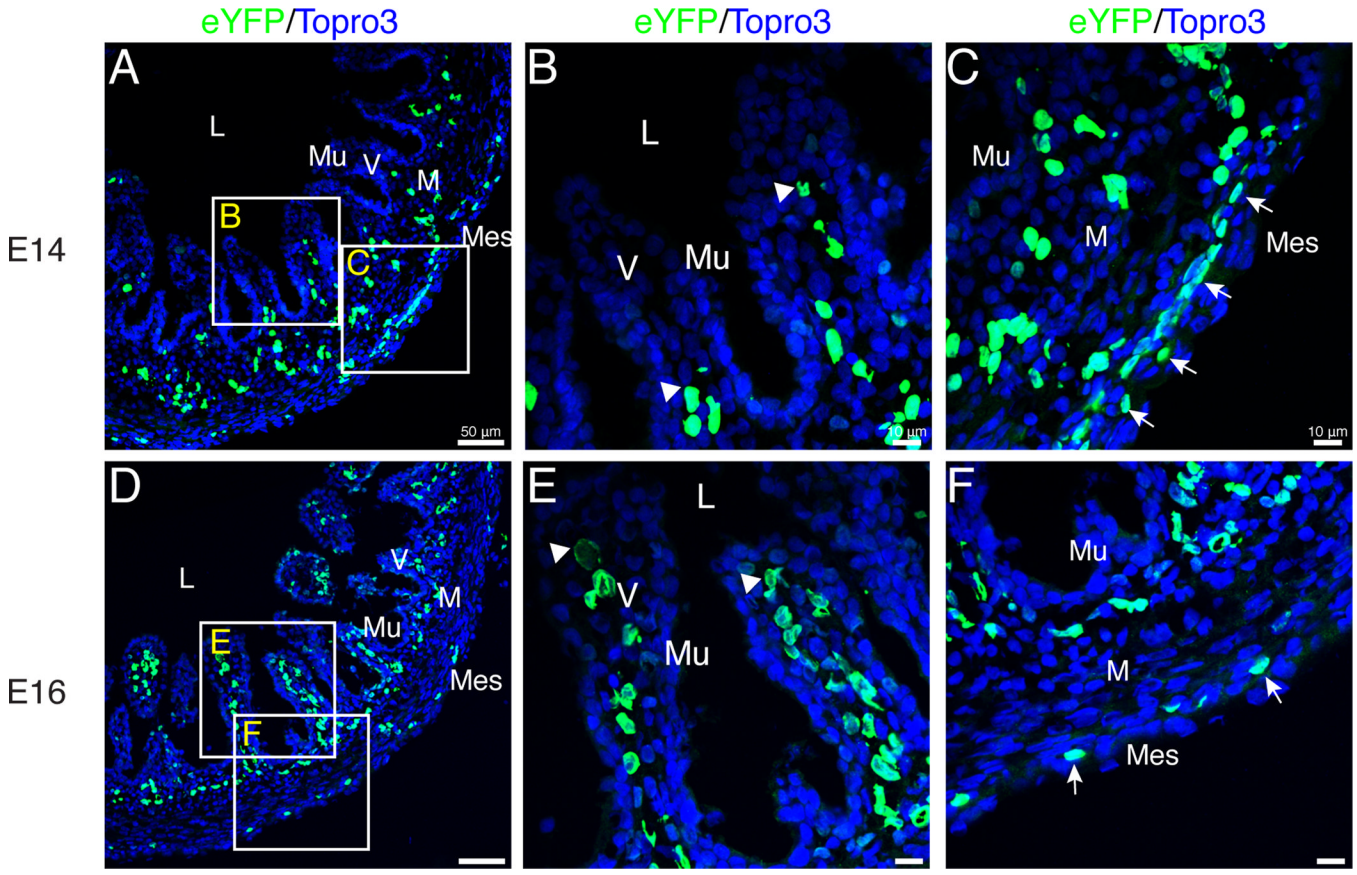

Figure 9. Extension of endothelial cells into the villi

Images are of sections through Tg(*tie1*:H2B-eYFP) quail intestines. **A–B**: At E14, eYFP-positive endothelial cells (arrowheads) were localized within the base of the villi in low numbers. **C**: The outer endothelial plexus was substantial at E14 (arrows). **D–E**: By E16, endothelial cells had reached the tip of the villi (arrowheads) and were present in high numbers. **F**: Thinning of the outer endothelial plexus was observed (arrows). Scale bars: 50µm (A, D), 10µm (B–C, E–F). L, lumen; M, mesenchyme; Mes, mesothelium; Mu, mucosa; V, villi.

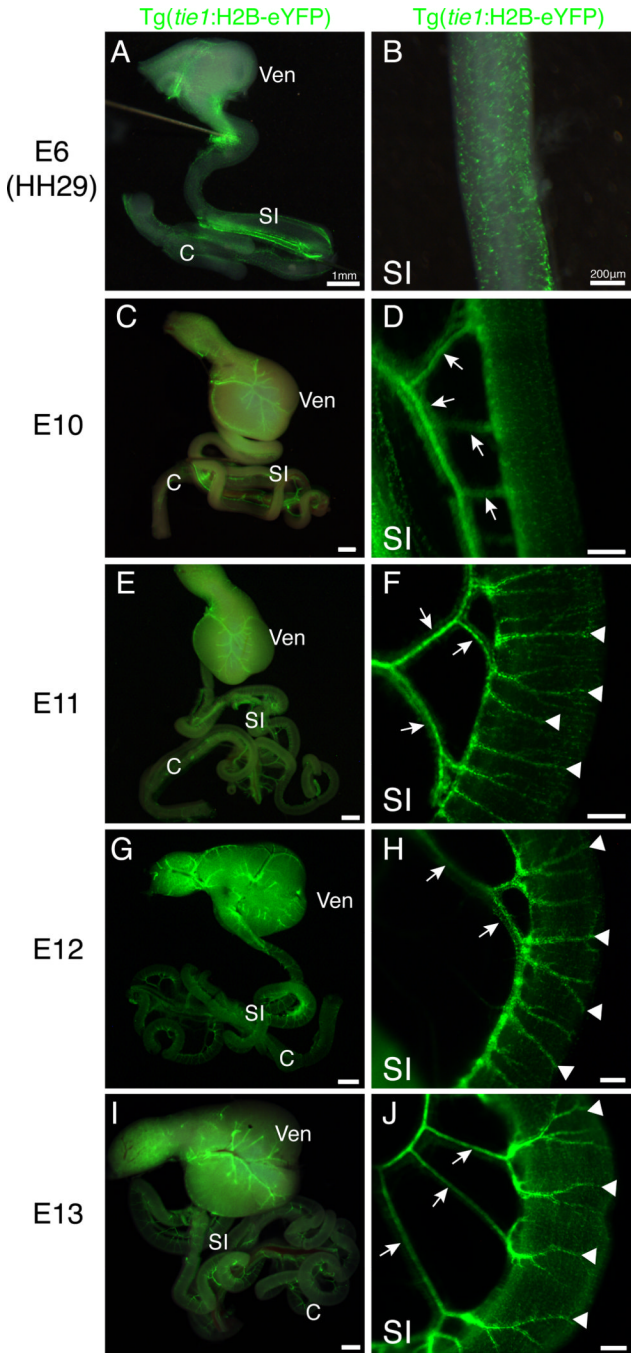

Figure 10. Development of large blood vessels of the small intestine

All panels are whole mount images of eYFP fluorescence in isolated gut tubes from Tg(*tie1*:H2B-eYFP) quail. **A–B**: At E6, eYFP-positive endothelial cells were evident in the wall of the small intestine in a honeycomb pattern. **C–D**: At E10, mesenteric vessels were visible (arrows) but large vessels on the small intestine proper were not observed. **E–F**: At E11, major vessels near the surface of the small intestine were present (arrowheads) extending from the mesentery (arrows). **G–J**: Major small intestinal vessels (arrows) displayed further branching at E12 and E13 (arrowheads). Scale bars: 1mm (A, C, E, G, I); 200μm (B, D, F, H, J). C, caeca; SI, small intestine; Ven; ventriculus.

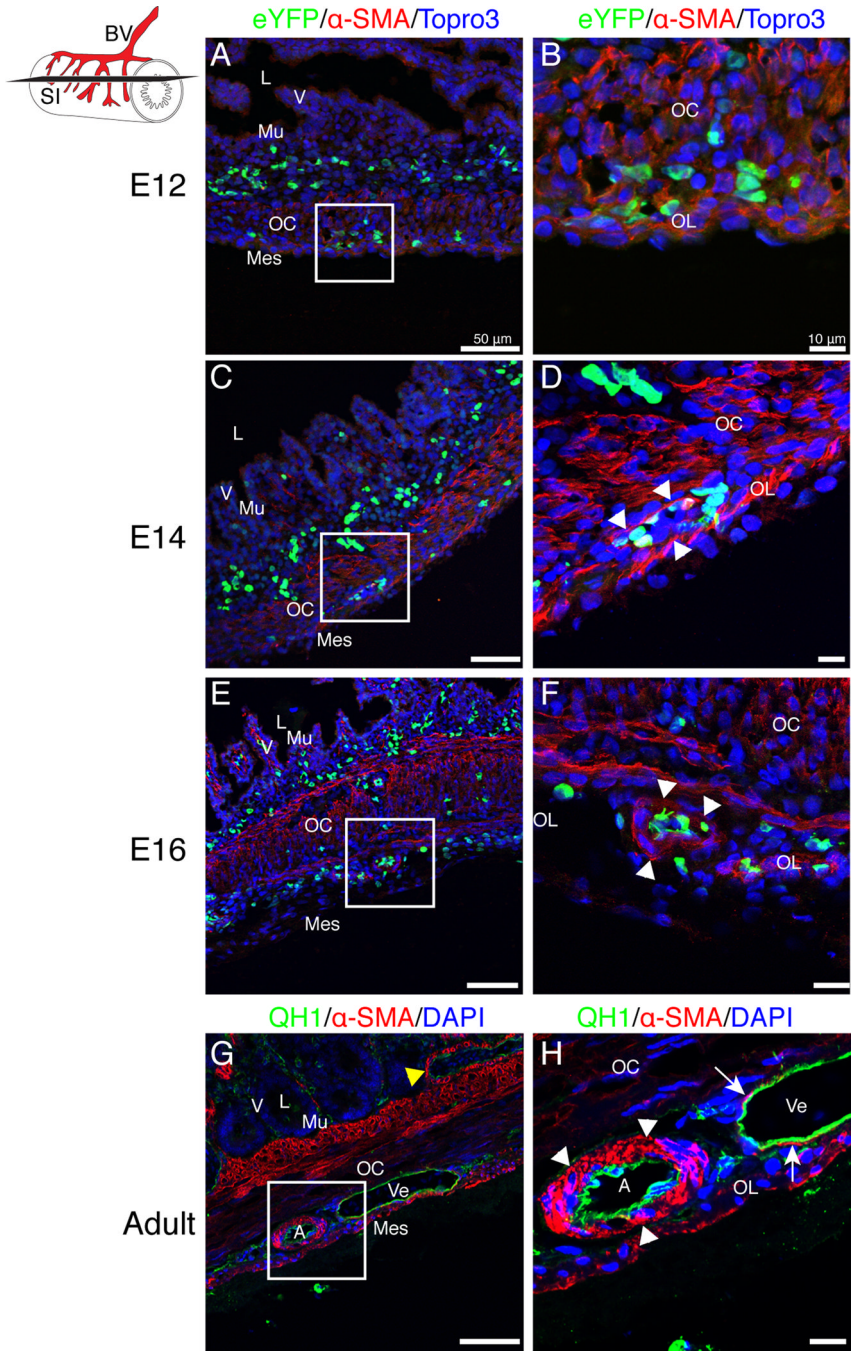

Figure 11. Muscularization of small intestinal blood vessels

Schematic in upper-left corner represents the small intestine (SI), blood vessels (BV) and the orientation of sections (black slice). A–F: Sections from Tg(*tie1*:H2B-eYFP) intestines. **A–B**: At E12, eYFP-positive endothelial cells subjacent to the coelomic surface were in close proximity to the visceral smooth muscle layers (OC, OL) but were not invested by vascular smooth muscle cells. **C–D**: At E14, vascular smooth muscle cells (α-SMA-positive, arrowheads) arranged in a single layer were identified surrounding eYFP-positive endothelial cells localized near the coelomic surface of the small intestine. **E–F**: At E16, the vascular smooth muscle cells appeared more mature and were in multiple layers surrounding

endothelial cells (arrowheads). **G–H**: QH1 staining of a wild type adult quail small intestine revealed mature vessels with multiple layers of vascular smooth muscle cells in large arteries (arrowheads) but only a single layer in veins (arrows). The second tier of blood vessels at the base of the villi was also muscularized in the adult (yellow arrowhead). Scale bars: 50μm (A, C, E, G) and 10μm (B, D, F, H). A, artery; L, lumen; Mes, mesothelium; Mu, mucosa; OC, outer circular muscle layer; Ve, vein; V, villi.

Table 1

Key stages and pivotal developmental events that occur throughout quail intestine development

E1.9 (HH12)	**E2.2 (HH16)**	**E3.5 (HH21)**	**E4 (HH23)**	**E5 (HH27)**	**E6 (HH29)**
• Continuous outer basement membrane • Narrow mesenchymal space • Single layered endothelial plexus • Open gut tube (GT)	• Dispersed outer basement membrane • Scattered mesenchymal cells • Single endothelial plexus • Open GT	• Continuous outer basement membrane • Multilayered mesenchyme • Peak in mesenchymal width • Stratified outer epithelium • Anterior and posterior closure of GT	• Continuous outer basement membrane • Contraction of mesenchymal width • Single layered outer epithelium	• Dispersed outer basement membrane • Increased mesenchymal width • Cytokeratin-positive outer epithelium	• Continuous outer basement membrane • Decreased mesenchymal width • Mesothelium • Completely closed GT • Endothelial plexus splits into two layers • Outer circular muscle layer • Length: 6mm
E10	**E11**	**E12**	**E14**	**E16**	
• Villi present • Outer longitudinal muscle layer • Absence of SMA-negative submesothelial mesenchyme • Length: 42mm	• Large surface blood vessels	• Sharp increase in mesenchymal area • Length: 72mm	• Endothelial cells in base of villi • Myofibroblasts in lamina propria • Inner circular muscle layer • Single layer of vascular smooth muscle • Length: 85mm	• Endodermal basement membrane dispersed • Endothelial cells in tips of villi • Inner longitudinal muscle layer • Multilayered vascular media • Limited submucosal mesenchyme • Length: 110mm	